INTELEC 09 - 31st International Telecommunications Energy Conference

October 18-22, 2009, Songdo Convensia, Incheon, Korea

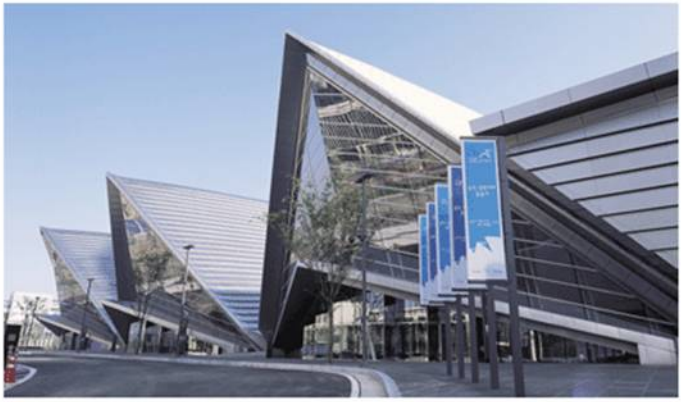

Organized by

KIEE(The Korean Institute of Electrical Engineers)

Technical Co-sponsorship

IEEE PELS (IEEE Power Electronic Society)

IEICE (The Institute of Electronics, Information and Communication Engineers)

IEEJ (The Institute of Electrical Engineers of Japan)

KIPE (The Korean Institute of Power Electronics)

Electric Machine and Drives (Poster Presentation) Oct, 21, 2009 (Wed,) 10:30-12:00

10:30-12:00 · PEM-1
Re-acceleration Characteristics of Stationary Discontinuous Armature Permanent Magnet Linear Synchronous Motor by Using Each Control System
Yong-Jae Kim, Kyoung-Pil Cho, Seung-Ho Shin, Youn-Ok Choi, Geum-Bae Cho (Chosun University, Korea)

10:30-12:00 · PEM-2
Development of IPM Synchronous Motor for Diesel Hybrid Electric Vehicle
Ju-Hee Cho, Hong-Seok Oh, Sang-Uk Cho, Deok-Geun-Kim (Komotek Co,. Ltd, Korea), Ik-Seong Park (LIGNex1 Co., Ltd, Korea)

10:30-12:00 · PEM-3
The Velocity Control of a Permanent Magnet Type Stepping Motor Using a Self-tuning Theory
Sung-Ho Hong, Soo-Rang Lee, Sung-Hwan Choi (R&D Center CU Medical Systems, Inc,, Korea), Young-Tae Kim, Sang-Don Lee (Kangnung Wonju National University, Korea), Cherl-Jin Kim (Halla University, Korea)

10:30-12:00 · PEM-4
Double-layer Rotor Design for Improving Characteristics of Single-phase LSPM Motor
Byeong-Hwa Lee, Fangliang, Jung-Pyo Hong (Hanyang University, Korea), Hyuk Nam (LG Electronics, Korea)

10:30-12:00 · PEM-5
Output Voltage Control of a Synchronous Generator for Ships Using Compound Type Digital AVR
Sang-Hoon Park, Seung-Kyung Lee, Su-Won Lee (Sungkyunkwan University, Korea), Jae-Sung Yu (HYOSUNG Heavy Industries Co,. Ltd,. Korea), Sang-Seuk Lee (PACTECH, Korea), Chung-Yuen Won (Sungkyunkwan University, Korea)

10:30-12:00 · PEM-6
Optimization of Magnetic Suspension Using Response Surface Methodology
Ho-Kyoung Lim, Jae-Woo Jung, Jung-Pyo Hong (Hanyang University, Korea)

10:30-12:00 · PEM-7
Novel Position Sensorless Starting Method of BLDC Motor for Reciprocating Compressor
Dae-Kyong Kim, Duck-Shik Shin (Korea Electronics Technology Institute, Korea), Sang-Taek Lee (Korea Electronics Technology Institute, Hanynag University, Korea), Hee-Jun Kim, Byung-Il Kwon (Hanynag University, Korea), Byung-Taek Kim (Kunsan National University, Korea), Kwang-Woon Lee (Mokpo National Maritime University, Korea)

10:30-12:00 · PEM-8
Optimal Design for Cogging Torque Reduction in BLDC Motor Using the Response Surface Method
Young-Kyoun Kim, Jung-Moo Seo, Seung-Bin Lim, Se-Hyun Rhyu, In-Sung Jung (Kore Electronics Technology Institute, Korea), Jin Hur (University of Ulsan, Korea)

10:30-12:00 · PEM-9
Core Loss Distribution of Three-Phase Induction Motor Using Numerical Method
Jeong-Jong Lee, Soon-O Kwon, Jung-Pyo Hong (Hanyang University, Korea), Ji-Hyun Kim, Kyung-Ho Ha (POSCO, Korea)

10:30-12:00 · PEM-10
Minimization of Torque Ripple in a BLDC Motor Using an Improved DC Link Voltage Control Method
Jin-soek Jang, Byung-taek Kim (Kunsan National University, Korea)

10:30-12:00
Finite Element Analysis of a Very Large-Scale Permanent Magnet BLDC Motor Considering Two-dimensional Magnetic Properties of Electrical Steels

Core Loss Distribution of Three-Phase Induction Motor Using Numerical Method

Jeong-Jong Lee[1], Soon-O Kwon[1], Jung-Pyo Hong[1], Ji-Hyun Kim[2], Kyung-Ho Ha[2]
[1] Department of Automotive Engineering, Hanyang Univ., Haengdang-dong, Seongdong-Gu, Seoul
[2] Electrical Steel Research Group, Technical Research Lab., POSCO, Korea
E-mail: motor@hanyang.ac.kr; hongjp@hanyang.ac.kr

Abstract — This paper presents core loss analysis of 3-phase induction motors used for industry applications. The core loss is affected by the time rate of the change of magnetic flux density. Generally core loss is spread out in stator and rotor core. And, rotor core loss is less than stator core because of constant field flux density of rotor. Tooth core loss density is large than yoke core loss because tooth has harmonic distortion of flux density. In this paper, transient finite element method used to analyze the magnetic flux density waveform in order to analysis the flux density according to varying time. Core losses in each element are evaluated using core loss curve tested by and Epstein test apparatus. Its result is shown the distribution of core loss density and partial thermal source.

I. Introduction

Three-phase induction motor wildly used for variety industry applications very much. This paper deals with the core-loss distribution of a 3-phase induction motor. Many studies on the core loss calculation have been conducted. In traditional ac machine theory the iron loss is viewed as being caused mainly by the fundamental frequency. Normally, under alternating flux conditions, the iron loss P_c in W/kg is separated into a hysteresis loss component P_h, and an eddy current component P_e, both in W/kg, as shown in (1).

$$P_c = P_h + P_e = k_h f B_m^{\alpha} + k_e f^2 B_m^2 \quad (1)$$

where f and B_m are the frequency and the peak value of the magnetic flux density, respectively. k_e, k_h and α are constants provided by the manufacturer. This conventional method assumes sinusoidal variation of the magnetic flux density waveforms. Therefore, this method is not sufficiently accurate because the magnetic flux density waveforms are non-sinusoidal. In order to take into account the harmonic effects of the magnetic flux density waveforms on iron losses, accurate prediction of the magnetic flux densities throughout the stator and the rotor cores need to be performed.

In many study, it is difficult to calculate the core loss because of local flux density and non-linear characteristic [1]. Many studies discussed lumped parameter for calculate core loss. In order to calculate core loss distribution, flux density of each element is calculated based on FEA. And, core loss of each element is obtained by the harmonic distribution and measured core loss data. Because the iron loss is affected by the time rate of the change of magnetic flux density at the motor cores, it is important to calculate the quantitative magnetic flux density distribution in the magnetic material. Therefore, the core loss is evaluated by the frequency analysis of the magnetic flux density distribution by the time-stepping FEM and the iron loss curves, which are provide by manufacturer. The harmonic analysis is used to analyze the magnetic flux density waveform in each element model. Iron losses in each element are evaluated using iron loss curves and total iron losses are obtained by the summation of the losses in all elements. Finally, the simulation results by the presented method are verified by the experimental results.

II. Analysis Method for Core Losses

A. Analysis Model

Fig. 1 and Table I show the half cross-section and brief specifications of the analysis model. The model consisted of 4 pole, 24 slot and squirrel cage with 34 bars.

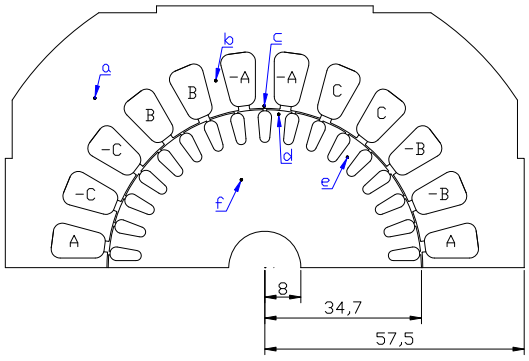

Fig. 1. Analysis model

TABLE I
Brief Specifications of 3-Phase Induction Motor

Item	Value	Item	Value
Phase number	3	Pole number	4
Input voltage (V_{LL})	100	Rated current (Arms)	1.59
Output (W)	133.5	Rated speed (rpm)	1350
Rated slip	0.1	Connection	Y

B. Finite Element Methods

Generally, Time-stepping FEM is used for the analysis of the magnetic field. The governing equation for 2-D FE analysis is given by (1).

$$\frac{\partial}{\partial x}\left(\frac{1}{\mu}\frac{\partial A}{\partial x}\right)+\frac{\partial}{\partial y}\left(\frac{1}{\mu}\frac{\partial A}{\partial y}\right)=\sigma\frac{dA}{dt}-J_0 \quad (1)$$

where A is the z-component of magnetic vector potential, μ is the permeability, σ is the conductivity of the materials and J_0 is the exciting current density of the stator winding.

The voltage equation per each phase can be written by (2).

$$V_a = I_a R_a + (L_a + L_m)\frac{dI_a}{dt} + \frac{d\phi_a}{dt} \quad (2)$$

where V_a, R_a and ϕ_a are the input voltage, the resistance and the flux linkage of each phase, respectively. L_a is the magnetizing inductance and L_m is the winding leakage inductance calculated by equivalent method [6]. The sum of L_a and L_m is the phase inductance.

For the time-stepping FEM, time step is fixed and the input voltage is defined at each time step.

C. Magnetic flux density of each step

The flux density can be calculated by FEM. In this paper, moving line technique is used to express rotor motions. The magnetic flux density of each element of each step is memorized to the files.

D. Coreloss calculation of each element

Fig. 2 shows the flow chart for the iron loss calculation. The temporal and the spatial variations of the magnetic flux density waveforms are calculated by performing time-stepping FEM. Spectrum analysis is used for the frequency analysis of the magnetic flux density at each element of the finite element (FE) analysis model. The iron losses $P_{ce}{}^{i}$ at each element are calculated from the summation of the losses $P_{cev}{}^{i}(B_v, vf)$ according to frequencies using DFT and iron loss curves. Finally, the total iron loss P_c is obtained by the summation of the iron losses in all the elements.

E. Measurement of 50PN1300 coreloss

Under no load conditions and depending on the motor, magnetic loading can be around 1.5 T, and increases with loading conditions. Some motors inherently operate at near saturation and at high frequencies. Of an apparatus used for the measurement of magnetic properties of samples of magnetic sheet material, a part in which the sample, in the form of stacks of uniform flat rectangular strips, is arranged in a closed magnetic circuit around the sides of a square, each side being equipped with test windings which surround the loss measurements. This methods is defined as "Epstein Test Method"[2]. In this paper, Epstein test method is used for sheet coreloss according to magnetic flux density and frequency. Fig. 3 shows the coreloss density measured by Epstein tester.

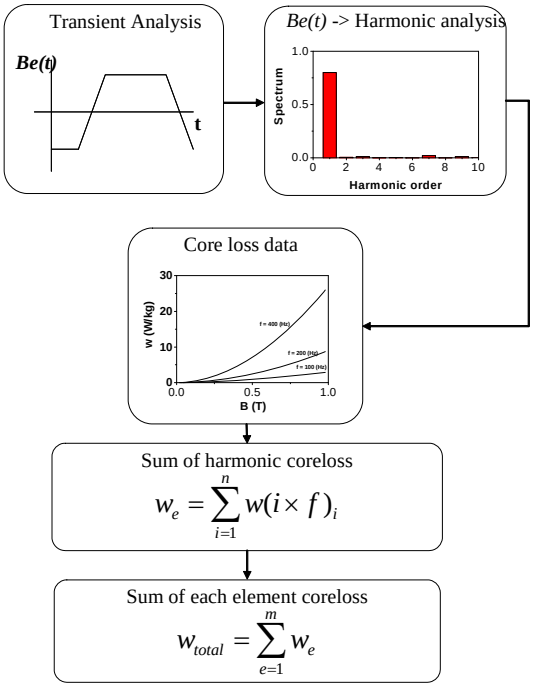

Fig. 2. Process for calculate the coreloss.

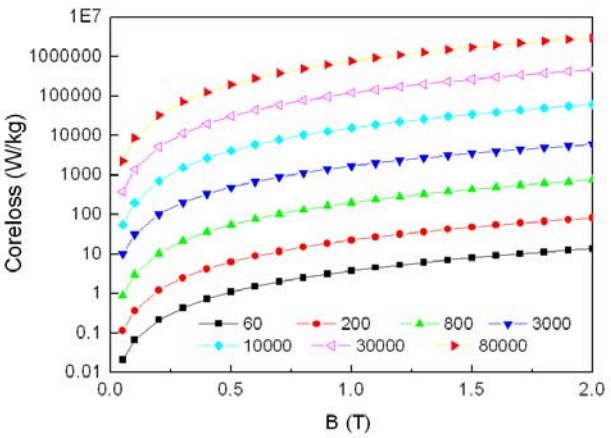

Fig. 3. Coreloss density measured by Epstein tester

III. Result & Discussions

A. Current waveform of the analysis model

Fig. 4 shows the simulated result of current waveform of each phase from initial time to stable statues. Slip of simulation is 0.1, the speed is 1350rpm. The rated current by simulation is similar to design parameter shown in table I. Fig. 5 shows the conductor loss of secondary with squirrel cages. The conductor loss of Fig. 5 is sum of each conductor loss of the analysis model. In this simulation, the conductivity is compensated to $8.66*10^6$ (S/m) which is 14% of pure copper conductivity. At the stable states, the conductor loss is very smaller than transient statues. Fig. 6 shows the equi-potential line according to simulation time. The magnetic flux density couldn't spread to inside of conductor bars at fig 6(a) because sudden current variation is effect on secondary conductor bar. The conductor bar is shaped the induced field against to

primary in the rotor. When the current is reached at the point PA in Fig.4, the equi-potential line is shown in Fig. 6(b).

Fig. (7) shows the magnetic flux density at the rated current.

B. Flux density variation of element

According to position of stator & rotor, the flux density is shown in Fig. 8 ~ Fig .12 of a~f of fig.1.

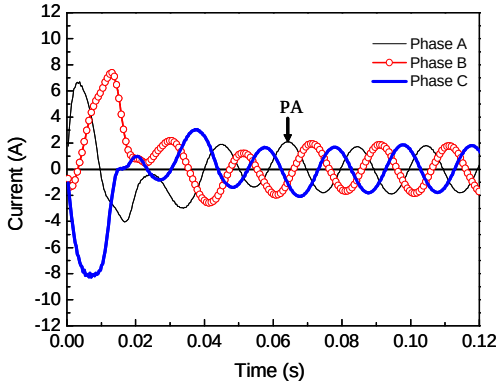

Fig. 4. Current waveforms by FEM analysis

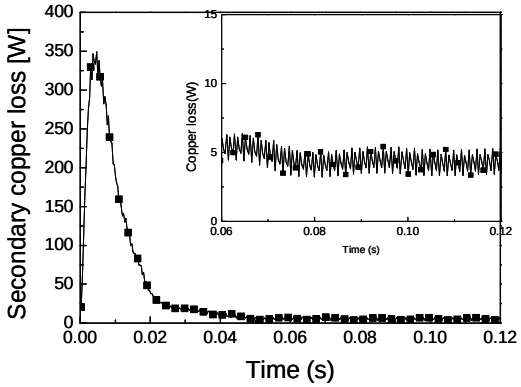

Fig. 5. Secondary conductor loss

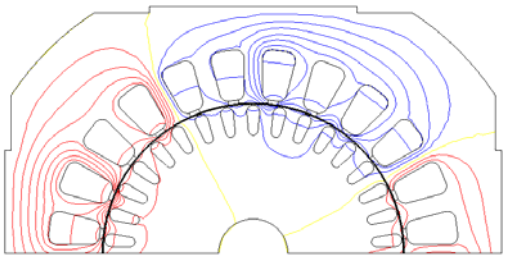

(a) equi-potential line of initial time

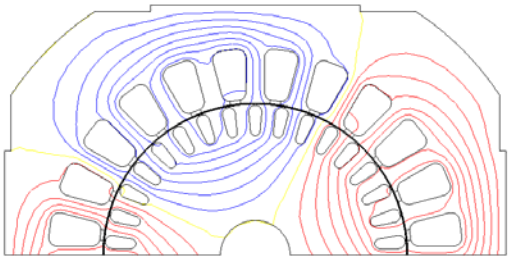

(b) equi-potential line @ time=0.063s

Fig. 6. Equi-potential according to simulation time

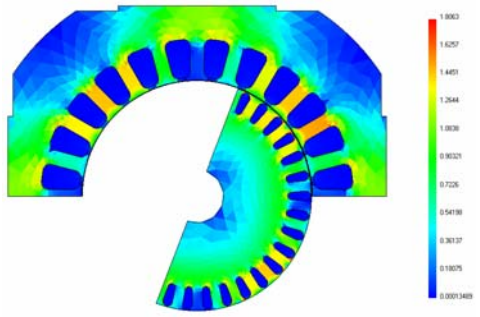

Fig. 7. Magnetic flux density at rated current

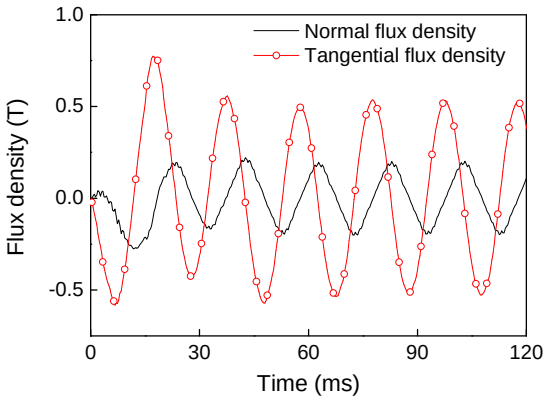

Fig. 8. Flux density of stator yoke in Fig. 1(a)

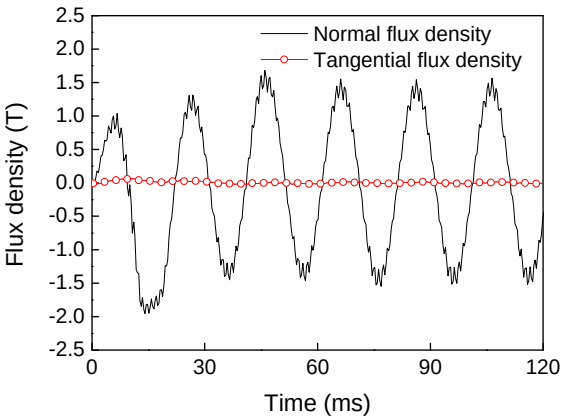

Fig. 9. Flux density of stator tooth in Fig. 1(b)

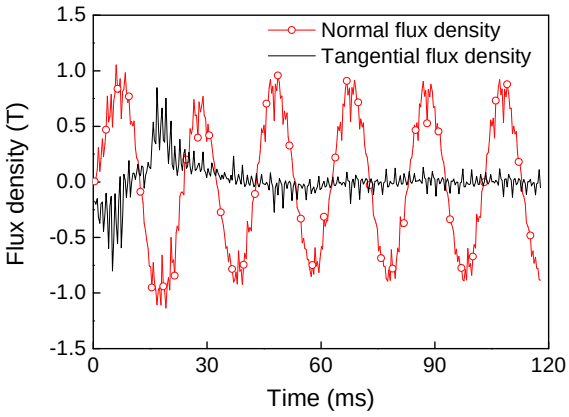

Fig. 10. Flux density of stator tooth edge of Fig. 1(c)

Fig. 8 are shown stator rotor yoke flux density. Teeth harmonic effect is disappear in yoke. Fig 10. and Fig 11 are shown at teeth edge respectively. Harmnic analysis result is shown in Fig. 13 and Fig. 14. In Fig. 13, the 18th harmonic order is caused teeth effect.

C. Core loss density distribution

Fig. 15 shows the distribution of core loss at rating point. In the edge of rotor core region have higher core loss density than stator core region. The test result shows in Table II. In the test, it is difficult of the coreloss and secondary copper losses to separate. Therefore it is compared with sum of coreloss and copper loss.

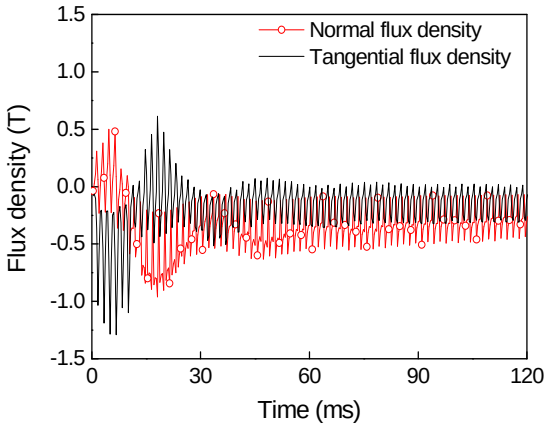

Fig. 11 Flux density of rotor tooth edge in Fig. 1(d)

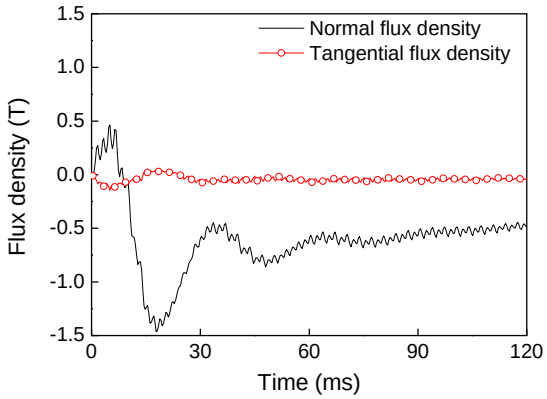

Fig. 12. Flux density of rotor teeth in Fig. 1(e)

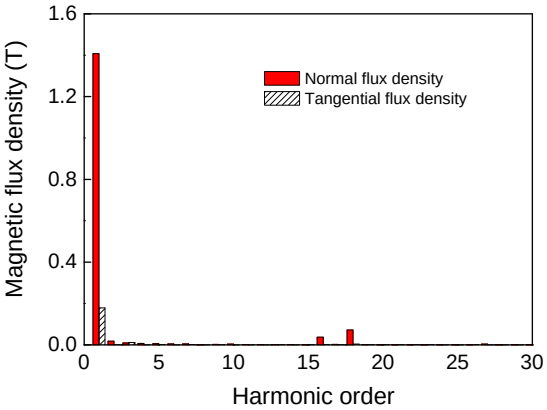

Fig. 13. Flux density harmonic order of stator teeth

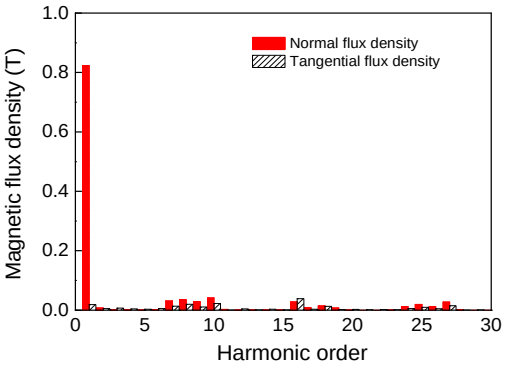

Fig. 14. Flux density harmonic order of stator teeth edge

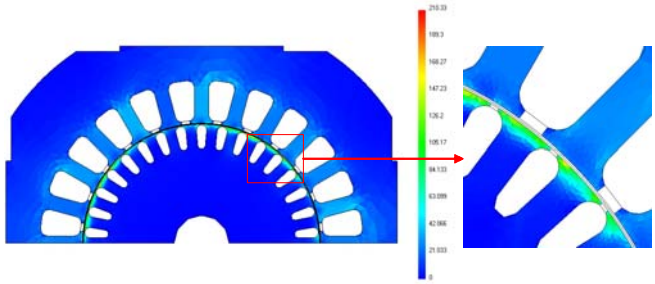

Fig. 15. Coreloss density of three phase induction motor (W/kg)

TABLE II
TESTED RESULTS OF THREE-PHASE INDUCTION MOTOR

Item	Value
Test Speed (rpm)	1489
Core material	50PN1300 (POSCO)
Simulation harmonic order	100
FEA core and conductor loss (W)	23.1
Experiment core and conductor loss (W)	21.6
Error (%)	6.5

IV. CONCLUSIONS

This paper presents the loss distribution of 3-phase induction motor fed by sinusoidal voltage using time-stepping FEM. The core loss is evaluated by the frequency analysis of the magnetic flux density distribution by the time-stepping FEM and the iron loss curves, which are provide by manufacturer. The harmonic analysis is used to analyze the magnetic flux density waveform in each element model. In the result, the flux density of regional flux density is displayed. The teeth coreloss density is more higher than yoke. Especially, in the teeth edge, there is high flux variation is occur the core losses. The results are compared with the experimental results.

REFERENCES

[1] H. Nam, K. H. Ha, J. J. Lee, J. P. Hong, and G. H. Kang, "A studcy on iron loss analysis method considering the harmonics of the flux density waveform using iron loss curves tested on Epstein samples," *IEEE Trans. Magn.*, vol. 39, no. 3, pp. 1472-1475, May 2003.

[2] K. E. Blazek and C. Riviello, "New magnetic parameters to characterize cold-rolled motor lamination steels and predict motor performance," IEEE Transactions on Magnetics, vol. 40, no. 4, pp. 1833– 1838, July 2004.